Easy Preparation of Tannin-Based Ag Catalysts for Ethylene Epoxidation

Sébastien Schaefer, Adrian Ramirez, Reyes Mallada, Maria T Izquierdo, Jesus Santamaria, Alain Celzard, Vanessa Fierro

Easy Preparation of Tannin-Based Ag Catalysts for Ethylene Epoxidation

Dr. Sébastien Schaefer [a], Dr. Adrian Ramirez [b,d], Dr. Reyes Mallada [b,d], Dr. Maria T. Izquierdo [c], Prof. Jesus Santamaria [b,d], Prof. Alain Celzard [a], Dr. Vanessa Fierro*[a]

Abstract: Ultramicroporous carbons loaded with silver (Ag) nanoparticles were synthesised by submitting tannins to hydrothermal treatment in aqueous solutions of silver nitrate at different concentrations, followed by a pyrolysis step. The resultant materials were oxidised with dioxygen diluted in argon for removing the carbon partly coating the Ag nanoparticles and thus increasing the active metal surface area. Morphological, chemical, structural and textural characterisations were carried out in order to establish relationships between the physicochemical properties of the materials and their performances as catalysts for ethylene epoxidation. The latter reaction was increasingly promoted at higher silver content, and the efficiency of the oxidative post-treatment was evidenced. The relation between selectivity and Ag content was nonlinear, in favour of the improved availability of silver nanoparticles after the removal of the carbon coating, at constant surface area and micropore size distribution of the carbon support. A favourable effect of Ag nanoparticles agglomeration on the selectivity was suggested.

Introduction

Ethylene epoxide (EO) is a widely used molecule for several applications such as medical disinfection and polymer synthesis, i.e., polyethyleneglycol [1, 2]. In the industry, ethylene epoxidation usually involves flowing ethylene and oxygen throughout a heated bed of Ag-based catalysts. The latter are essentially made of low-surface area porous alumina decorated with Ag nanoparticles [3]. The reason of using Ag is mainly due to both its good selectivity and the relative stability of Ag_2O surface when compared to those of other metallic oxides like Cu_2O or Au_2O [4]. Indeed, Cu_2O exhibits a much lower selectivity than Ag_2O for ethylene epoxidation, whereas Au_2O is less stable than Ag_2O in reaction conditions [4]. Still, Cu appears to have better selectivity to EO than Au [5]**.** Other metals such as Ni, Pt or Pd lead to the total combustion of EO [6]. The high worldwide demand of EO, together with the need of saving reagents and avoiding heavy purification steps, require highly selective catalysts [3].

[a] Dr. S. Schaefer, Prof. A. Celzard, Dr. V Fierro
Insitut Jean Lamour – UMR 7198
CNRS-Université de Lorraine
27 rue Philippe Séguin, BP 21042, 88051 Épinal cedex 9, France
E-mail: vanessa.fierro@univ-lorraine.fr
[b] Dr. A. Ramirez, Dr. R. Mallada, Prof. J. Santamaria
Instituto de Nanociencia de Aragón
Department of Chemical and Environmental Engineering
Universidad de Zaragoza
Campus Río Ebro, Edif. I+D, C/ Mariano Esquillor Gómez, s/n, 4. Zaragoza. E-50018, Spain
[c] Dr. M.T. Izquierdo
Instituto de Carboquímica
Consejo Superior de Investigaciones Científicas - CSIC
C/ Miguel Luesma Castán, 4. Zaragoza. E-50018, Spain
[d] Networking Research Center on Bioengineering, Biomaterials and Nanomedicine (CIBER-BBN)
C/ Monforte de Lemos, 3-5 Pabellón 11, 28029 Madrid, Spain

Ethylene and oxygen can react through either a direct, Eley-Rideal type, or a non-direct mechanism, Langmuir-Hinshelwood type [3]. In the case of the non-direct mechanism, the reagents and the metallic catalyst form an oxometallacycle (OMC) intermediate, eventually promoting the formation of acetaldehyde as by-product, thus decreasing the selectivity [3]. The 110 face would have the best catalytic properties due to a better OMC adsorption [7]**.** Maintaining a high oxygen coverage on Ag nanoparticles surfaces prevents the anchorage of the non-selective OMC intermediate and allows switching from this non-direct to a direct mechanism that is much more selective [3, 8, 9]. But, as silver oxide is not totally stable in the reaction conditions, it is necessary to avoid oxygen vacancies by using agents able to block them. Thus, in order to enhance the selectivity of the reaction, the role of Ag-doping agents and adatoms like caesium or chlorine, added as co-reagents to the gas, were theoretically and experimentally investigated and showed their capabilities to enhance the catalysts selectivity [10-12]. Moreover, promoters such as Cl increase the electrophilic nature of the adsorbed oxygen, due to the difference of electronegativity between the adsorbed oxygen and chlorine. Thus, under those experimental conditions, the adsorbed oxygen atoms are more likely to open the C-C bound and to form the EO ring [12]. Such enhanced catalyst systems are mainly bi-metallic systems of Ag nanoparticles supported on copper oxide [10, 11, 13]. In order to achieve EO synthesis in mild conditions, some authors proposed Nd-loaded catalysts and hydrogen-peroxide as oxidative agent [14]. If the most common supports are Al_2O_3 and SiO_2, layered double hydroxides have been also used [15, 16]**.**

The results presented herein have to be considered as an early investigation exploring the possibility of using a biosourced carbon matrix as support for Ag nanoparticles. Besides, we showed that the corresponding carbon-silver hybrid materials can be obtained by a one-pot, green and easy process. For that purpose, commercial tannin extracts derived from Mimosa tree (*Acacia Mearnsii*) were used as carbon source. Tannins were indeed already proved to be a cheap, non-toxic and excellent precursor for preparing a quite broad range of porous carbons, from aerogels to rigid foams passing through monoliths having various cellular structures for a number of applications [17-25]. Submitting tannins to hydrothermal carbonisation (HTC) at mild temperatures, typically from 403 to 523 K, under self-generated pressure, produces hydrochar microspheres whose further pyrolysis leads to carbon microspheres having various structures and compositions [26-29]. For instance, HTC of tannin in ammonia allowed the production of N-doped hydrochars [30] and, in the presence of dissolved $AgNO_3$, Ag-loaded hydrochars could be prepared in a one-pot process [31]. The pyrolysis of the latter hydrochars led to the formation of microporous carbons with Ag nanoparticles embedded in the carbon matrix [31].

In the present study, we modified the method previously used to prepare Ag-carbon nanocomposites[31]. After hydrochar pyrolysis, a mild oxidative post-treatment was applied to remove part of the carbon potentially coating Ag nanoparticles and to promote the reactivity of Ag nanoparticles.

Results and Discussion

Morphology and structure

All carbon materials from both CX and OCX series were very fine black powders. TEM observations allowed determining three types of structures in the final materials. The biggest particles, having average diameters within the 3.5 – 7 µm range, were based on carbon microspheres (**Figure S1.a)**). Their strong agglomeration, however, prevented a more accurate evaluation of their individual sizes. Such kind of structure is commonly observed for hydrochar-derived carbons [27, 30-34], and is due to both nucleation and growth mechanisms taking place in the liquid medium [27, 32]. As already observed for saccharides and other biosourced precursors [22, 35-38], tannins must probably also undergo a complex reaction sequence comprising hydrolysis, dehydration and condensation steps, leading to nucleation and growth processes [32, 36]. On some images and using the appropriate magnification, some rare and small (0.5 – 1 µm) isolated micro-particles could indeed be observed, in favour of such mechanisms.

The second type of structure, presented in **Figure S1.b)** and **S1.c)**, was made of Ag nanoparticles coated with carbon. Those nanoparticles could be classified in two different categories: 1) small or unitary nanoparticles, and 2) big agglomerates. The small nanoparticles had a spheroidal morphology and an average size mainly within the 50 – 300 nm range. The average size slightly increased with the amount of silver in the initial solution. The agglomerates were much bigger, reaching 500 nm and even 1 µm for the largest ones, and presented ill-defined shapes.

The third type of structure was made of much smaller Ag nanoparticles (20 – 50 nm) somewhat aggregated and bearing a thin carbon coating, but still remaining individualised (**Figure S1.d)**). Some of those nanoparticles had a cubic shape, revealing the cubic structure of Ag and the monocrystalline nature of the smallest nanoparticles. Due to the high overlapping of the silver nanoparticles, it was not possible to obtain reliable particle size distribution and average particle size using TEM imaging.

The three aforementioned types of structures could be observed in all materials of the CX series, with negligible differences from one sample to another. The partial removal of the carbon coating from the Ag nanoparticles in the OCX series confirmed the effective action of the oxidative treatment. Comparing C8 and OC8 materials (**Figures 1.a), 1.c)** and **1.b), 1.d**) respectively) evidenced that the carbon coating, formerly covering an important part of all nanoparticles, became much thinner or even disappeared after the treatment.

Carbon microspheres and the Ag nanoparticles (types 2 and 3) were in contact with each other but never mixed homogeneously. No Ag nanoparticles were indeed inside spherical carbon microparticles, suggesting that Ag nanoparticles were formed by a different mechanism from that of nucleation and growth. After oxidation, Ag nanoparticles looked bigger. This can be explained either by carbon removal leading to a reduction of the space between the nanoparticles, i.e., by agglomeration or by aggregation, due to sintering.

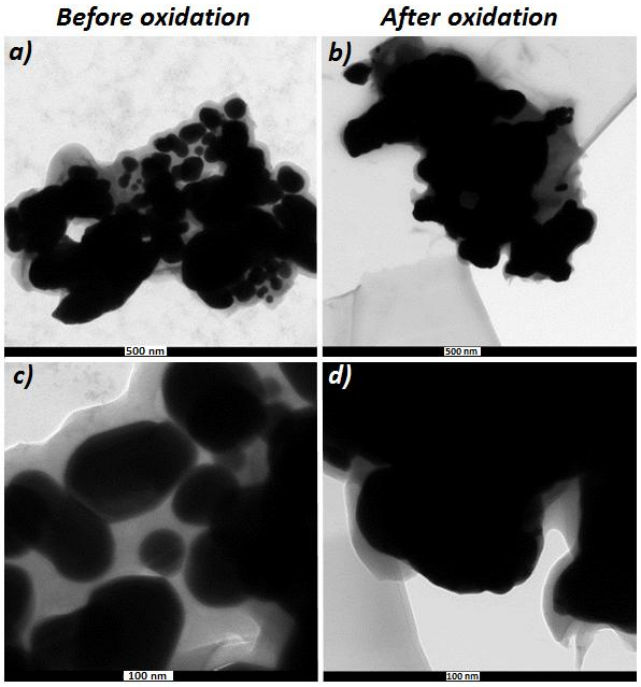

Figure 1. TEM images showing the C16 material ((a) and (c)) and the OC16 material ((b) and (d)).

XRD patterns were obtained for all the materials, but only two examples are shown in **Figure S2** for the C16 and OC16 samples. The volume-weighted mean column height calculated from the integral breadth was taken to obtain the average crystallite size (LVol-IB in **Table S1**). Apart from this, all the lattice parameters were in the 408.5-408.6 pm range (less than 0.05% of difference) and hence very close to the typical value of pure crystalline Ag, 408.6 pm. This finding suggests that the present Ag nanocrystals have a nearly perfect fcc structure (JCPDS No. 04-0783), irrespective to the Ag content and to the application of an oxidative treatment or not. All crystallographic data can be found in **Table S1**.

Silver content

Finding a correlation between Ag content and catalytic performances was essential to have an idea of the suitability of the catalyst. **Figure 2** shows that a linear relationship exists between the final Ag content in carbon materials and the initial amount of 0.1 M $AgNO_3$ solution introduced in the autoclave. It was already shown that, during HTC, nucleation and growth

rates of carbonaceous particles depend on tannin concentration [27]: the higher the concentration, the faster the nucleation. In the CX series, the Ag contents were 2.12, 2.18, 4.82 and 9.12 wt. % of the total mass of catalyst (carbon plus Ag) for C2, C4, C8 and C16, respectively. After oxidation, the Ag contents increased to 2.66, 3.68, 6.15 and 11.92 wt. % for OC2, OC4, OC8 and OC16, respectively. The increase of the Ag content after oxidation is readily explained by the removal of part of the carbon initially coating the silver particles. Removing carbon coatings after use is an important concern for most catalysts used in the petrochemical industry, and especially in reforming processes, since the carbon deposits hinder the access of reactants to the active sites of the catalyst, thus causing a loss of catalytic activity. The removal of carbon coatings from such catalysts is called regeneration and is mainly carried out with air, O_2, CO_2, H_2O or H_2 treatment under heating in different partial pressure and temperature conditions (e.g. in the typical range of temperature 573-873 K for O_2) [39, 40]. Herein, this regeneration process was mimicked in order to activate the catalyst and to enhance its performances. The limited gasification of the carbon support and the carbon coatings on the Ag nanoparticle surface led to an increase of the overall Ag content.

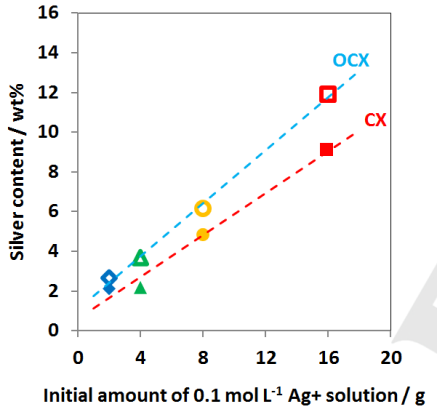

Figure 2. Silver content in the CX and OCX series of samples as a function of the initial amount of 0.1 M $AgNO_3$ in the HTC solution (◆ C2, ◇ OC2, ▲ C4, △ C4, ● C8, ○ OC8, ■ C16, □ OC16).

Figure 3 shows the increase of the average crystallite size with the silver content. The Ag crystallite sizes for the CX and OCX sets of materials were very similar except for C16 and OC16 samples, which could be explained by the heterogeneity of the C16 material. The increase of the crystallite size when silver content increased is due to the higher rates of both nucleation and growth of silver nanoparticles during the synthesis. As the crystallite size was almost constant before and after the oxidation step, it can be concluded that no real aggregation, or sintering, occurred during the oxidation step. The increase of the nanoparticles size, observed on TEM pictures, would be more likely due to simple agglomeration, which not changes the nanoparticles structure.

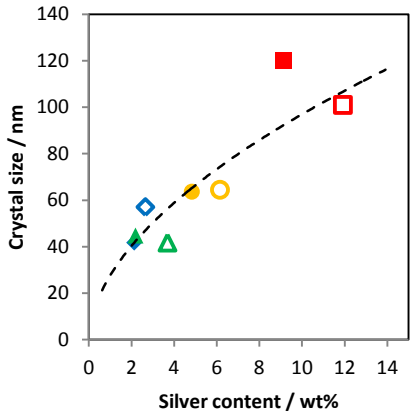

Figure 3. Ag crystallite size versus Ag content. The dashed line is just a guide for the eye (◆ C2, ◇ OC2, ▲ C4, △ C4, ● C8, ○ OC8, ■ C16, □ OC16).

Textural analysis and water adsorption properties

The observations of the N_2 adsorption isotherms at 77 K (**Figure S3 a)** and **c)**) show that all materials were essentially microporous (typical pore size lower than 2 nm). Indeed, all the isotherms were type I and exhibited a very narrow knee, characteristic of ultramicroporous materials, and a horizontal plateau without hysteresis, which indicates the absence of significant mesoporosity (typical pore size within the range 2-50 nm). Plateau positions were almost identical for all the materials, suggesting the very similar pore textures of those materials. CO_2 adsorption isotherms are shown in **Figure S3.b)** and **d)**), all were comparable in shape and adsorption capacities evidencing the high similitudes in ultramicroporous texture of all the materials.

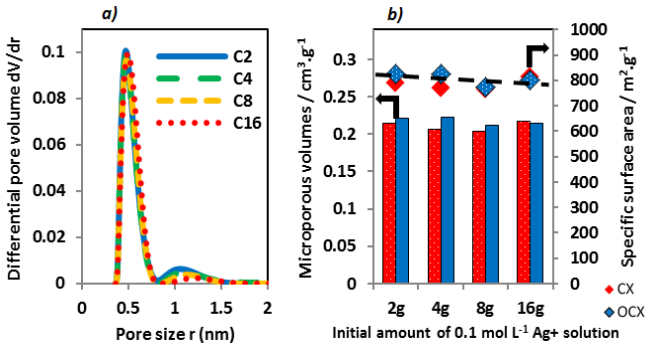

Figure 3. (a) PSDs of the CX series, (b) Microporous volumes, specific surface areas and average micropore sizes for the CX and OCX series of samples (line is a guide for the eyes). Values were obtained using the NLDFT model (SAIEUS software) applied to N_2 (77K) and CO_2 (273K) adsorption isotherms.

Opposite to N_2 adsorption isotherms, the shape of CO_2 adsorption isotherms does not allow making direct assumptions about the textural characteristics of the material but only gives information on the narrow porosity (< 1 nm) and on the existence

of diffusional limitations at 77 K. Pore size distributions (PSDs) were obtained by treating both N_2 and CO_2 isotherms using the SAIEUS® software. The PSDs of the materials from the CX series are given in **Figure 3.a)**. No porosity was detected above 2 nm, confirming the exclusively microporous character of the materials. The PSDs were bimodal with peaks typically centred in the ranges of supermicropores (0.7-2 nm) and ultramicropores (<0.7 nm). The same conclusions apply to the materials from the OCX series (**Figure S4**). Integrating the PSDs allowed calculating specific surface areas, microporous volumes and average micropore sizes of all materials. Most of the porous volume (i.e., more than 81%) corresponded to ultramicropores. The oxidative treatment slightly developed the pore texture. Indeed, the average specific surface area of the OCX series was 806 $m^2 g^{-1}$, i.e., 2 % higher than that of the CX series, 784 $m^2 g^{-1}$. Although this effect might be attributed to a classical activation of carbon, similar to what can be obtained by using CO_2 or H_2O at high temperature [41], it remains in the typical range of the analysis error of volumetric adsorption devices. Such small difference is thus not expected to play a role in catalytic performances. Moreover, the average micropore sizes were around 0.54 nm for all materials. The details of textural properties can be found in **Table 2**.

Table 2. Textural properties of the materials from the CX and OXC series.

	BET surface area / $m^2 g^{-1}$	NLDFT surface area / $m^2 g^{-1}$	Microporous volume / $cm^3 g^{-1}$ [a]	Percentage of ultra-micropores / vol. % [b]	Average micropore size / nm [a]
Before oxidation					
C2	528	789	0.214	85.3	0.54
C4	511	770	0.206	81.4	0.54
C8	502	764	0.203	90.4	0.53
C16	536	814	0.217	92.7	0.53
After oxidation					
OC2	551	824	0.221	91.2	0.54
OC4	549	825	0.223	90.0	0.54
OC8	520	775	0.211	78.2	0.59
OC16	529	800	0.214	88.7	0.54

[a] From the PSDs obtained by NLDFT treatment of the N_2 and CO_2 adsorption isotherms
[b] Obtained from ratio of the ultramicroporous volume (I<0.7 nm) to the total pore volume

Water adsorption isotherms at 295.13 K were type V, according to the IUPAC classification, characteristic of materials having poorly hydrophilic properties [42] (see **Figure 4.a)** for one representative example and **Figure S5** for other materials) and were very similar for all materials, in agreement with their similar textural properties. Differences between them might therefore be exclusively attributed to the surface chemistry or functional groups on the surface. Those isotherms allowed determining the apparent affinity constants of the materials for water. Such constants correspond to the slope of the linear part ($P/P^0 < 0.15$) of the adsorption isotherms (see the inset in **Figure 4.a)** for example). The increase of Ag content led to a decrease of affinity constants (approximatively from 70 to 50), see **Figure 4.b)**). As noticed above, the carbon in which Ag nanoparticles were embedded seemed to follow a formation path different from that of pure carbon microspheres. The carbon microspheres would indeed be, according to several authors [32, 38], formed by a diffusion process leading to the more hydrophilic nature of the outer layer containing oxygenated functions. The more hydrophilic nature of the outer carbon, compared to the carbon inside the microspheres, would be maintained after pyrolysis.

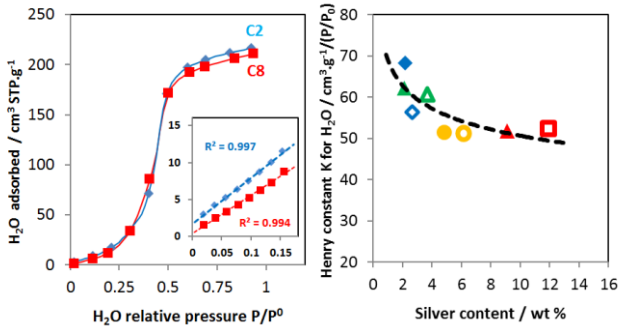

Figure 4. (a) Water adsorption isotherms for the C2 and C16 materials (the inset is a zoom at low relative pressure), and (b) water affinity coefficients obtained from low-pressure, linearized water adsorption at 313.15 K onto all the materials (◆ C2, ◇ OC2, ▲ C4, △ C4, ● C8, ○ OC8, ■ C16, □ OC16).

It can be assumed that increasing the silver content or carrying out the oxidative treatment decreases the hydrophilic fraction of the carbon microspheres. The silver nanoparticles are indeed embedded in a carbon coating having followed a totally different formation path than that of carbon microspheres, and also having a less hydrophilic nature. As the oxidative treatment removed the outer part of the carbon particles, it also removed the more hydrophilic part of the carbon microspheres. Silver is indeed known to be a catalyst of carbon oxidation [43, 44]. Moreover, the moderate changes of textural properties within the whole set of materials (less than 10% in terms of microporous volume, see again **Figure 3.b)**) cannot explain the variations of Henry's constant (as high as 33 %, see **Figure 4**). In addition, there are no correlations between the small changes of textural properties and the water adsorption properties. Thus, the significant decrease of Henry's constant observed as a function of silver content can only be explained by related changes of surface chemistry and hydrophilic character of the carbon material.

Ethylene epoxidation

Figure 5.a) shows the selectivity as a function of the conversion rate. Temperature had a negative effect on selectivity but a positive effect on conversion rate, in good agreement with the literature [3, 11].

As for the effect of silver content, the more Ag was present, the higher was the selectivity and, to a lesser extent, the higher was the conversion rate. Increasing the amount of Ag in the catalyst thus logically led to an improvement of the catalytic properties. In addition, the materials of the OCX series presented higher catalytic performances than their non-oxidised counterparts.

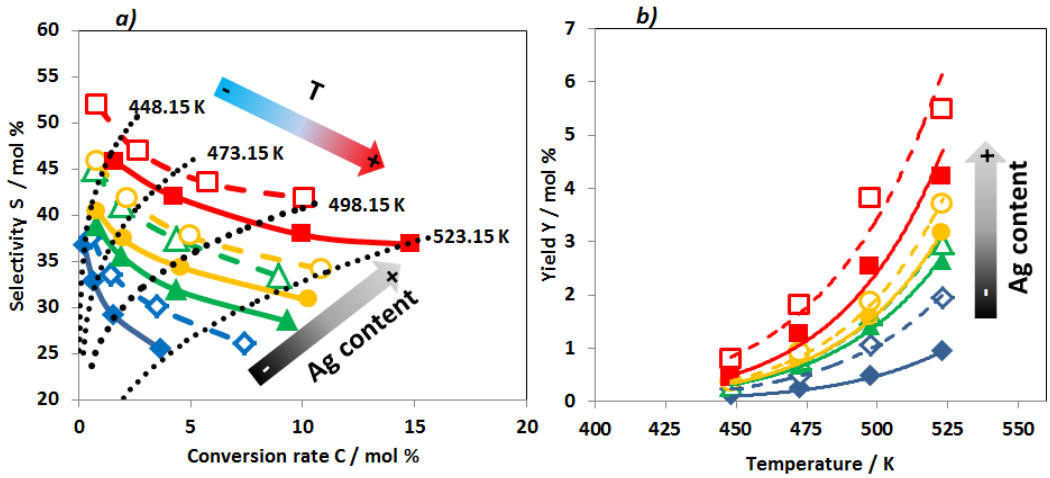

Figure 5. (a) Selectivity of the catalyst versus conversion rate at 4 different temperatures, and (b) reaction yield versus temperature for the two series of samples CX and OCX. The lines are just guides for the eye (◆ C2, ◇ OC2, ▲ C4, △ C4, ● C8, ○ OC8, ■ C16, □ OC16).

The latter finding was explained by the increase of the Ag content, by a better accessibility due to the removal of the carbon coating, and by the increase of the particle's size, in agreement with a former study [45].The increase of the particle size might be due to an agglomeration phenomenon occurring during oxidation but also to the removal of the carbon coating. Both agglomeration and carbon removal led to higher active surface and to enhanced catalytic properties through a higher selectivity. **Figure 5.b)** shows that the total reaction yield increased with temperature. This trend can be explained by the fact that the increase of conversion yield was high enough to compensate the decrease of selectivity. This assumption is clearly supported by **Figure S6**, where the first derivatives of selectivity and conversion were plotted versus temperature and combined to give the first derivative of the total yield versus temperature.

The highest values of selectivity, conversion rate and total yields were reached for the C16 and OC16 materials, containing 9.1 and 11.9 wt. % of Ag, respectively. It is worth comparing the present materials with those synthesised by Jankowiak and Barteau [10, 13], having similar Ag contents (i.e., 11-13 wt. % of Ag) and which exhibited a 3.06 mol. % conversion (at 500 K) and a selectivity close to 49.5 mol. % (at 490 K) when tested with an O_2/ethylene molar ratio equal to 2 (at a total pressure of 1.34 bar). C8 and OC8 exhibited selectivity values equal to 37.9 and 43.5 mol. % (at 498.15 K), respectively, and conversion rates equal to 9.99 and 5.77 mol. % (at 498.15 K), respectively. Thus, our materials presented similar or higher performances under comparable experimental conditions.

The effect of Ag content on the selectivity of the catalysts is presented in **Figure S7**. As noticed above, the selectivity increased with Ag content but the trend was not linear. The selectivity increase cannot be due to an increase of Ag surface area but most likely to an increase of Ag nanoparticle size. Figure 6 shows the effect of the oxidative treatment on the selectivity at the same temperatures as in **Figure 6**.

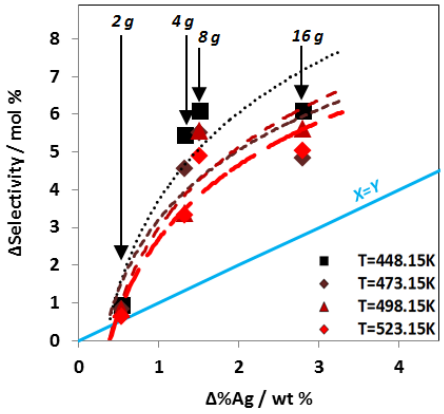

Figure 6. Comparison of oxidised materials (OCX) with respect to non-oxidised ones (CX) expressed as the corresponding increase of selectivity versus increase of silver content. The arrows point materials synthetized with a given amount (g) of initial 1mol L^{-1} of $AgNO_3$ solution. Lines are just guides for the eye.

The selectivity increase (ΔSelectivity) of oxidised samples with respect to non-oxidised ones was presented here versus the Ag

increase (Δ%Ag, see again Eq. (1)) measured after materials' oxidation at initial constant silver loading in the HTC solution.
The relation between selectivity and Ag content was, again, non-linear. This finding supports the improved availability of silver nanoparticles after the removal of the carbon coating, at constant surface area and micropore size distribution of the carbon support. The increase of the size of the Ag nanoparticles, after the oxidative treatment, explains the higher selectivity. The oxygenated functions, accounting for the hydrophilic character of the material, were assumed to be only located on the carbon surface, not on the Ag nanoparticles. Thus the catalytic properties of the materials in terms of conversion, selectivit y and yield, were only correlated with the Ag content of the materials and to the size of the Ag nanoparticles.
Figure 7 shows that the increase of the crystallite size led to an increase of selectivity. Even if crystallite size is not equal to nanoparticle size (quite uneasy to determine from TEM images), we can assume that both sizes follow the same behaviour. After the oxidative treatment, the crystallite sizes of the CX and OCX series were very similar. Thus, the increase of the selectivity after the oxidative treatment was not due to the growth of silver crystallites by aggregation but to the removal of the carbon coating, which increased the silver active *surface*. Indeed, the increase of silver nanoparticles agglomeration (not aggregation) during oxidation might also explain the increase of selectivity.

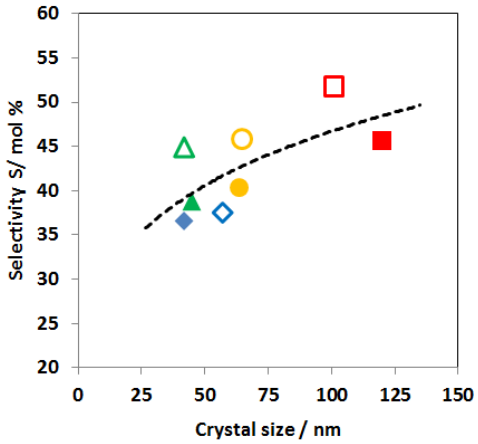

Figure 7. Selectivity of EO reaction at 448.15 K versus crystallite size for the two series of samples CX and OCX. The lines are just guides for the eye (◆ C2, ◇ OC2, ▲ C4, △ C4, ● C8, ○ OC8, ■ C16, □ OC16).

Figure 8 shows the selectivity to EO and conversion obtained with OC16, which exhibited the highest catalytic performances in this study, together with those showed by materials prepared by Jankowiak and Barteau[10], based on an Ag/Al_2O_3 catalyst. The later reference material showed much lower selectivity to EO than OC16 at similar experimental conditions. Doping with Cs, Cu or treatment with chloride promoted selectivity to EO, leading us to conclude on the promising catalytic enhancement of tannin-based Ag catalysts.

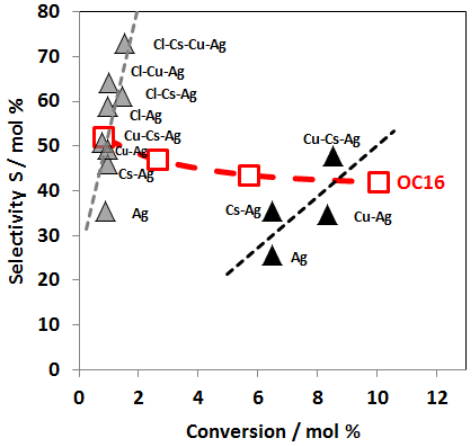

Figure 8. Comparison between OC16 □ (P=1bar, T = 448-523 K, C_2H_4/O_2=2) and materials from Jankowiak and Barteau.[10] ▲ (P=1.34 bar, T=540 K, C_2H_4/O_2=1); ▲ (P=0.4 bar, T=479-540 K, C_2H_4/O_2=2). Ag stands for the reference material while Cs, Cu or/and Cl in the label stand for metal doping or chlorine treatment.

Conclusion

Carbon materials decorated with silver nanoparticles as potential catalysts for ethylene epoxidation were synthesised using a green precursor through an innovative process. The hydrothermal treatment of mimosa tannins dissolved in a solution of silver nitrate produced hydrochars which, after subsequent pyrolysis, led to porous carbons loaded with silver nanoparticles.
TEM observations evidenced two populations of Ag nanoparticles, partly coated with carbon: big agglomerates (50 - 300 nm) and small or elementary nanoparticles (20 - 50 nm). An oxidative treatment allowed removing part of such carbon layer without impact on size and structure of silver particles, as seen by XRD. Besides, varying the Ag content changed neither the surface area (average around 800 $m^2\ g^{-1}$) nor the average pore size (average around 0.54 nm) of the carbon support. Therefore, whether the materials were oxidised or not, differences in the performances of the materials used as catalysts for ethylene epoxidation were expected to be only due to the silver present at the carbon surface.
Water adsorption experiments suggested that the higher was the Ag content, the less hydrophilic the materials were. This effect was explained by the partial removal of the outermost hydrophilic layer of the carbon microspheres.
The increase of reaction temperature led to a decrease of selectivity but also to an increase of conversion. The latter compensated favourably the former, leading to an increase of total yield with temperature. The oxidative treatment increased the Ag content but the selectivity was improved in a much higher extent, which was explained by the increase of Ag apparent particle size due to agglomeration and carbon removal occurring during the oxidation step. Finally, the materials exhibited similar or even better catalytic properties compared to other silver-based materials reported in literature. Further improvement for

Supporting Information Summary

Supporting information provides experimental details about materials synthesis and characterization. **Figure S1** shows additional information about the morphology of the materials. The morphology of the spherical carbon microparticles can be observed in **Figure S1.a)** while **Figure S1.b)**, **c)**, **e)**, and **f)** show the typical morphology of the Ag nanoparticles of C2, C16 and OC16 materials. **Figure S1.d)** shows small Ag nanoparticles agglomerated in C8 material. **Figures S2.a)** and **b)** show the XRD patterns of C16 and OC16 materials. **Table S1** sums up the Ag-related XRD data for all the materials. **Figures S3.a)** and **b)** together with **Figures S3.c)** and **d)** show the N_2 and CO_2 adsorption isotherms for the CX and OCX series respectively. **Figure S4** shows the pore size distributions of the OCX series. **Figures S5.a)** and **b)** show the water adsorption isotherms for the CX and OCX series. **Figure S6** shows the first derivatives of selectivity (S), conversion (C) and total yield (Y) versus temperature for C2 material. **Figure S7** shows the evolution of selectivity with the Ag content for all the materials.

Acknowledgements

The authors gratefully acknowledge the financial support of the CPER 2007-2013 “Structuration du Pôle de Compétitivité Fibres Grand’Est” (Competitiveness Fibre Cluster), through local (Conseil Général des Vosges), regional (Région Lorraine), national (DRRT and FNADT) and European (FEDER) funds. Part of this work was supported by CHEERS project (FEDER funds).
Financial support from the Regional Government of Aragon (DGA) is gratefully acknowledged. TEM measurements were performed in the Laboratorio de Microscopias Avanzadas (LMA) at the Instituto de Nanociencia de Aragon (INA), Universidad de Zaragoza (Spain).

Keywords Carbon support, heterogeneous catalysis, hydrothermal treatment, silver, tannins

References

[1] W. A. Rutala, D. J. Weber, *J. Hosp. Infect.* **1999**, 43, S43-S55.
[2] P. P. McClellan, *Ind. Eng. Chem.* **1950**, 42, 2402-2407.
[3] M. O. Ozbek, R. A. van Santen, *Catal. Lett.* **2013**, 143, 131-141.
[4] M. O. Ozbek, I. Onal, R. A. van Santen, *J. Catal.* **2011**, 284, 230-235.
[5] C.C. Lee, H.T. Chen, *J. Phys. Chem. C* **2016**, 120, 7646-7652.
[6] M. Mavrikakis, D. J. Doren, M. A. Barteau, *J. Phys. Chem. B* **1998**, 102, 394-399.
[7] L. Zhu, W. Zhang, J.Q. Zhu, D.J. Cheng, *Appl. Catal. A-General* **2017**, 538, 27-36.
[8] A. Kokalj, P. Gava, S. de Gironcoli, S. Baroni, *J. Phys. Chem. C* **2008**, 112, 1019-1027.
[9] M. O. Ozbek, I. Onal, R. A. van Santen, *Top. Catal.* **2012**, 55, 710-717.
[10] J. T. Jankowiak, M. A. Barteau, *J. Catal.* **2005**, 236, 379-386.
[11] A. Ramirez, J. L. Hueso, H. Suarez, R. Mallada, A. Ibarra, S. Irusta, J. Santamaria, *Angew. Chem. Int. Ed. Engl.* **2016**, 55, 11158-11161.
[12] T. C. R. Rocha, M. Havecker, A. Knop-Gericke, R. Schlogl, *J. Catal.* **2014**, 312, 12-16.
[13] J. T. Jankowiak, M. A. Barteau, *J. Catal.* **2005**, 236, 366-378.
[14] W.J. Yan, A. Ramanathan, P.D. Patel, S.K. Maiti, B.B. Laird, W.H. Thompson, B. Subramaniam, *J. Catal.* **2016**, 336, 75-84.
[15] F.Z. Zhang, X.F. Zhao, C.H. Feng, B. Li, T. Chen, W. Lu, X.D. Lei, S.L. Xu, *Acs. Catal.* **2011**, 1(4), 232-237.
[16] X.T. Wang, Z.Q. Liang, F.Z. Zhang, L. Yang, S.L. Xu, *J. Mater. Sci.* **2013**, 48(17), 5899-5903.
[17] N. Rey-Raap, A. Szczurek, V. Fierro, A. Celzard, J. A. Menendez, A. Arenillas, *Ind. Crop. Prod.* **2016**, 82, 100-106.
[18] L. I. Grishechko, G. Amaral-Labat, V. Fierro, A. Szczurek, B. N. Kuznetsov, A. Celzard*, Rsc. Adv.* **2016**, 6, 65698-65708.
[19] A. Szczurek, V. Fierro, A. Pizzi, A. Celzard, *Carbon* **2014**, 74, 352-362.
[20] A. Szczurek, V. Fierro, A. Pizzi, M. Stauber, A. Celzard, *Ind. Crop. Prod.* **2014**, 54, 40-53.
[21] A. Szczurek, G. Amaral-Labat, V. Fierro, A. Pizzi, E. Masson, A. Celzard, *Carbon* **2011**, 49, 2773-2784.
[22] A. Szczurek, G. Amaral-Labat, V. Fierro, A. Pizzi, A. Celzard*, Carbon* **2011**, 49, 2785-2794.
[23] M. Letellier, J. Macutkevic, A. Paddubskaya, A. Klochkov, P. Kuzhir, J. Banys, V. Fierro, A. Celzard, *Ferroelectrics* **2015**, 479, 119-126.
[24] M. Letellier, J. Macutkevic, A. Paddubskaya, A. Plyushch, P. Kuzhir, M. Ivanov, J. Banys, A. Pizzi, V. Fierro, A. Celzard, *IEEE T. Electromagn. C.* **2015**, 57, 989-995.
[25] D. Bychanok, A. Plyushch, P. Kuzhir, J. Macutkevic, M. Letellier, A. Szczurek, V. Fierro, A. Celzard, *IEEE International Conference on Microwaves, Communications, Antennas and Electronic Systems (Comcas)* **2015**.
[26] F. L. Braghiroli, V. Fierro, A. Szczurek, N. Stein, J. Parmentier, A. Celzard, *Ind. Crop. Prod.* **2015**, 70, 332-340.
[27] F. L. Braghiroli, V. Fierro, M. T. Izquierdo, J. Parmentier, A. Pizzi, A. Celzard, *Bioresource Technol.* **2014**, 151, 271-277.
[28] F. L. Braghiroli, V. Fierro, M. T. Izquierdo, J. Parmentier, A. Pizzi, A. Celzard, *Carbon* **2012**, 50, 5411-5420.
[29] F. Braghiroli, V. Fierro, A. Pizzi, K. Rode, W. Radke, L. Delmotte, J. Parmentier, A. Celzard, *Ind. Crop. Prod.* **2013**, 44, 330-335.
[30] F. L. Braghiroli, V. Fierro, M. T. Izquierdo, J. Parmentier, A. Pizzi, L. Delmotte, P. Fioux, A. Celzard, *Ind. Crop. Prod.* **2015**, 66, 282-290.
[31] F. L. Braghiroli, V. Fierro, J. Parmentier, L. Vidal, P. Gadonneix, A. Celzard, *Ind. Crop. Prod.* **2015**, 77, 364-374.
[32] C. Y. Chen, X. D. Sun, X. C. Jiang, D. Niu, A. B. Yu, Z. G. Liu, J. G. Li, *Nanoscale Res. Lett.* **2009**, 4, 971-976.
[33] M. Sevilla, A. B. Fuertes, *Carbon* **2009**, 47, 2281-2289.
[34] A. J. Romero-Anaya, M. Ouzzine, M. A. Lillo-Rodenas, A. Linares-Solano, *Carbon* **2014**, 68, 296-307.
[35] M. Sevilla, A. B. Fuertes, R. Mokaya, *Energ. Environ. Sci.* **2011**, 4, 1400-1410.
[36] X. Q. Fan, L. X. Zhang, G. B. Zhang, Z. Shu, J. L. Shi, *Carbon* **2013**, 61, 423-430.
[37] L. Zhao, N. Baccile, S. Gross, Y. Zhang, W. Wei, Y. Sun, M. Antonietti, M.-M. Titirici, *Carbon* **2010**, 48, 3778-3787.
[38] M. Sevilla, A. B. Fuertes, *Chem-Eur. J.* **2009**, 15, 4195-4203.
[39] C. H. Bartholomew, *Appl. Catal. A-General* **2001**, 212, 17-60.
[40] M. D. Argyle, C. H. Bartholomew, Catalysts **2015**, 5, 145-269.
[41] K. Tomkow, T. Siemieniewska, F. Czechowski, A. Jankowska, *Fuel* **1977**, 56, 121-124.
[42] E. P. Ng, S. Mintova, *Micropor. Mesopor. Mat.* **2008**, 114, 1-26.
[43] P. S. Harris, F. S. Feates, B. G. Reuben, *Carbon* **1974**, 12, 189-197.
[44] D. W. McKee, *Carbon,* **1970**, 8, 623-635.
[45] S. N. Goncharova, E. A. Paukshtis, B. S. Balzhinimaev, *Appl. Catal. A-General* **1995**, 126, 67-84.

Ultramicroporous carbons loaded with silver (Ag) nanoparticles were synthesised by submitting tannins to hydrothermal treatment. The resultant materials were oxidised and used as catalyst for ethylene epoxidation. The relation between selectivity and Ag content was nonlinear, suggesting the improved availability of silver nanoparticles after the removal of the carbon coating, at constant surface area and micropore size distribution of the carbon support. A favourable effect of Ag nanoparticles agglomeration on the selectivity is suggested.